TECHNISCHE UNIVERSITÄT WIEN

DIPLOMARBEIT

Binding kinetics between the T cell receptor and its ligand pMHC

zur Erlangen des akademischen Grades

Diplom-Ingenieur/in

im Rahmen des Studiums

Biomedical Engineering

eingereicht von

Dominik Dungl
Matrikelnummer 01227400

ausgeführt am Institut für angewandte Physik
der Fakultät für Physik der Technischen Universität Wien

Betreuung
Betreuer: Univ. Prof. Dipl.-Ing. Dr. techn. Gerhard Schütz
Mitwirkung: Senior Scientist Dipl.-Ing. Dr. techn. Mario Brameshuber
Mitwirkung: Dipl.-Ing. Lukas Schrangl

Wien, 12.08.2019 (Unterschrift Verfasser/in) (Unterschrift Betreuer/in)

Zusammenfassung

Die Erkennung von Krankheitserregern durch den T-Zell-Rezeptor spielt eine entscheidende Rolle im Immunsystem. Die Bindungskinetik zwischen dem T-Zell-Rezeptor und seinem Liganden ist noch immer Gegenstand der Forschung. Sie wurde von Huppa u. a. [1] mithilfe von Fluoreszenzmikroskopie kombiniert mit Förster Resonant Energy Transfer (FRET) untersucht und sie fanden eine Dissoziationszeitkonstante von ungefähr 0.1 s. Im Gegensatz dazu fanden O'Donoghue u. a. [2] eine Dissoziationszeitkonstante von ungefähr 5 s unter Verwendung von Fluoreszenzmikroskopie mit langen Belichtungszeiten. In dieser Arbeit wurde versucht beide Resultate in Einklang zu bringen, indem man die Methoden beider Publikationen kombinierte, um die Bindungskinetik des T-Zell-Rezeptors mit ihrem Liganden zu messen. Experimentelle Verfahren wurden entwickelt und die Interaktion zwischen Rezeptor und Ligand mittels langer Belichtungszeit beobachtet. Die FRET-Experimente waren jedoch aufgrund ähnlicher Resultate in Negativkontrollen nicht aussagekräftig.

Abstract

The recognition of pathogens by the T cell receptor plays a crucial role in the immune system. The binding kinetics between the T cell receptor and its ligand are still debated. They have been characterized by Huppa et al. [1] using a fluorescence microscopy combined with a Förster Resonant Energy Transfer (FRET) based approach and reported off times of approximately 0.1 s. In contrast O'Donoghue et al. [2] reported different off times of approximately 5 s using fluorescence microscopy with long exposure times. In this thesis, it was attempted to reconcile both results by combining the methods of both papers to measure the binding kinetics of T cell receptors and its ligands. Experimental procedures were established and receptor–ligand interactions were observed using long exposures, but the FRET experiments were inconclusive due to similar results in negative control experiments.

Contents

Contents

1. Introduction

T cells, which are an integral part of the adaptive immune system, recognize pathogens with their T cell receptor (TCR). Each TCR identifies a specific peptide sequence presented by an antigen-presenting cell. The antigen-presenting cell displays the antigen via major histocompatibility complexes (MHC) on the cell membrane. Antigen recognition is very specific: Each T cell is only activated by a matching peptide-loaded MHC (pMHC). Other pMHC lead to reduced or no activation of the T cell. At the same time, the recognition process is also very sensitive, which means that it takes very few ligands to activate the T cell [3]. See Figure 1.1 for an illustration of a T cell and antigen-presenting cell interaction.

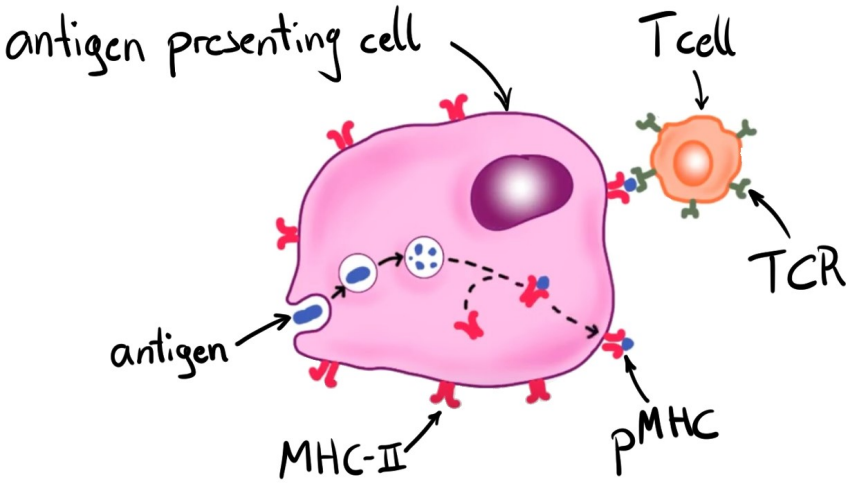

Figure 1.1.: Illustration of the interaction of an antigen-presenting cell with a T cell. The antigen-presenting cell digests antigens into peptides and loads them onto its surface-bound MHC-II protein. The T cell interacts with the peptide loaded MHC (pMHC) via its T cell receptor (TCR). Image modified from [4].

The interaction between a T cell receptor and pMHC is one of the most discussed subjects concerning the immune response. The mechanism of distinguishing different pMHC is not fully understood yet. According to the kinetic proofreading model [5] [6], the binding time of the pMHC to the TCR is important in order to allow for cytosolic kinases to phosphorylate internal structures of the TCR. Therefore the binding time between TCR and pMHC might be the decisive factor for antigen recognition. To further investigate the model, the binding dynamics of TCR and pMHC were examined in this thesis.

The studies by Huppa et al. [1] and O'Donoghue et al. [2] both measure the kinetic rate on very similar models by using different fluorescent microscopy methods. Huppa et al. [1] used FRET based fluorescence microscopy to measure the binding dynamics of the TCR and its ligand and concluded an off-time τ_{off} of approximately 100 ms. O'Donoghue et al. [2] measured the off-time with long exposure times and concluded a τ_{off} of approximately 5 s.

The aim of this thesis was to reproduce and reconcile the differences in the results of both methods by combining FRET and long exposure times to measure the kinetic binding times of TCR and pMHC.

To better compare and understand these conflicting papers and the method used for these T cell experiments, the basics are explained in this introduction chapter.

1.1. Immune system

The following introduction to the immune system was summarized from Murphy and Weaver [7].

After pathogens get past physical barriers, like the skin and mucous membranes, they encounter the two main strategies of the body against pathogens: the innate and the adaptive immune system. The innate immune system provides pattern recognition against many pathogens and does not change during life.

The adaptive immune system is specific to individual antigens and remembers previously encountered pathogens. It is the focus of the thesis.

1.1.1. Innate immune system

Macrophages, dendritic cells and neutrophils belong to the sensor cells of the innate immune system. They have many different pattern recognition receptors (PRRs) specific for a wide range of pathogen-associated molecular patterns (PAMPs) of microbes. These microbial structures are a good target, because they are conserved by evolution. With the help of PRRs, the innate immunes system recognizes PAMPs or the damage caused by pathogens to differentiate between self and foreign organisms.

For example, when bacteria trigger macrophages or neutrophils, they can release chemokines and cytokines into extra-cellular space. Chemokines are chemoattractants and cytokines affect the behaviour of nearby cells e.g. the permeability and stickiness of blood vessels. The increased permeability allows additional fluid and protein to pass into tissue and causes the typical redness, heat and swelling of inflammation. The increased stickiness helps additional immune cells like neutrophils or monocytes, precursors of macrophages, to stick to the wall of the blood vessel and migrate into the tissue towards the inflammation, attracted by the chemokines, where they help fight the bacteria.

1.1.2. Adaptive immune system

The cells of the adaptive immune system, the so-called lymphocytes, fall under two categories: B and T cells. Both progenitors of B and T cells come from the bone marrow, but the T cells mature in the thymus, whereas the B cells mature in bone marrow.

On their membranes they both have proteins as receptors, which recognize specific antigens. Due to random recombination of variable receptor genes and pairing of variable receptor protein chains, each lymphocyte recognizes a unique antigen. The number of different lymphocytes and therefore pathogens that can be recognized is extremely large. During maturation,

lymphocytes that are sensitive to antigens originating from the body are sorted out.

Lymphocytes circulate in the blood and peripheral lymphoid organs like lymph nodes, spleen and mucosal lymphoid tissues. Lymphocytes that have not yet been activated by an antigen, so-called naive lymphocytes, can recognize their particular antigen to become activated and differentiate into effector cells to defend the body.

B cell

Each B cell receptor recognizes a specific chemical structure and is similar to immunoglobulins or antibodies, but membrane bound. They are Y shaped, with a constant region partially inside the plasma membrane and a variable region binding to the antigen. Upon activation of the naive B cells, they differentiate into plasma cells and memory cells. Plasma cells produce antibodies with the same binding site as the naive B cell and secrete them into the blood stream, where they help fight against infections. Memory cells stay around long after the infection has passed and provide a long lasting immunity to the pathogen by generating an accelerated and more robust response the next time they encounter the pathogen. An illustration of the B cell is shown in Figure 1.2.

1.2. T cell

T cell receptors recognize only pathogen derived peptides bound to the major histocompatibility complex (pMHC). They interact not only with the presented peptide, but also with the polymorphic features of MHC for more specificity. Similar to the B cell receptors, they are membrane bound via a constant region and bind to pMHC with their variable region. See Figure 1.2 for an illustration. Naive T cells that have encountered their specific pathogen proliferate and produce many effector cells. There are different kinds of effector T cells: cytotoxic T cells, which kill cells afflicted

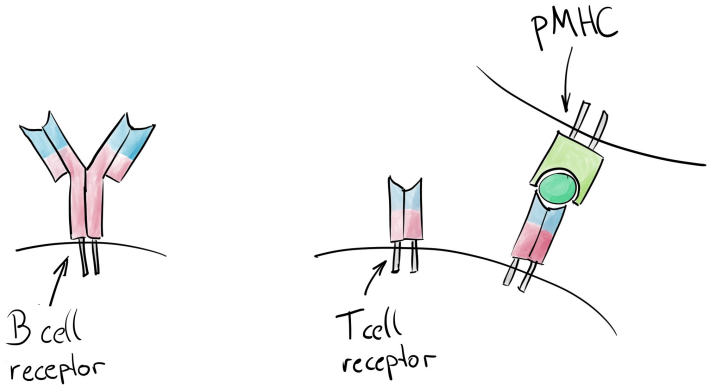

Figure 1.2.: Left: Illustration of a B cell receptor, which can bind to chemical structures of any kind. The antibodies produced by the B cell are similar but not membrane bound. Right: Illustration of a T cell receptor, which only binds to a peptide loaded MHC molecule.

by pathogens; helper T cells, which activate functions of other cells; regulatory T cells, which limit the possible damage of the immune response; and memory cells for long lasting immunity.

1.2.1. $CD8^+$ T cells

A subclass of T cells are the so-called $CD8^+$ T cells or killer T cells. CD8 is a transmembrane glycoprotein that acts as a co-receptor to the TCR on $CD8^+$ T cells. CD8 can bind to pMHC simultaneously with TCR to enhance the activation. TCR and CD8 recognize only class I MHC proteins, which are expressed on all cells in the body and present antigens derived from proteins in the cytosol of the infected cell, which may include pathogenic material. A $CD8^+$ T cell can kill the infected cell after recognizing the presented pMHC I complex on its cell surface.

1.2.2. $CD4^+$ T cells

$CD4^+$ T cells are a subclass of T cells also called helper T cells and support other effector cells. Like CD8, CD4 is a glycoprotein acting as a co-receptor

to the TCR and binds to pMHC simultaneously with the TCR. CD4 and TCR recognize only class II pMHC, which is mainly located on the surface of antigen presenting cells like dendritic cells, macrophages and B cells.

For example, a dendritic cell would ingest a pathogen at the site of infection and travel from there into the draining lymph node. The dendritic cell degrades the pathogen and presents its peptides on MHC class II molecules and other co-stimulatory receptors on its surface. The naive $CD4^+$ T cell recognizes the pMHC and activates, which leads to its proliferation. Daughter cells of the activated helper T cells then leave the lymph node. If a helper T cell encounters a B cell with the correct antigen MHC II molecule, it will influence the isotope of antibodies produced by the B cell by releasing cytokines. A macrophage with a correct pMHC II on its surface would trigger the T cell to release cytokines, aiding with the destruction of pathogens in the macrophage's vesicles.

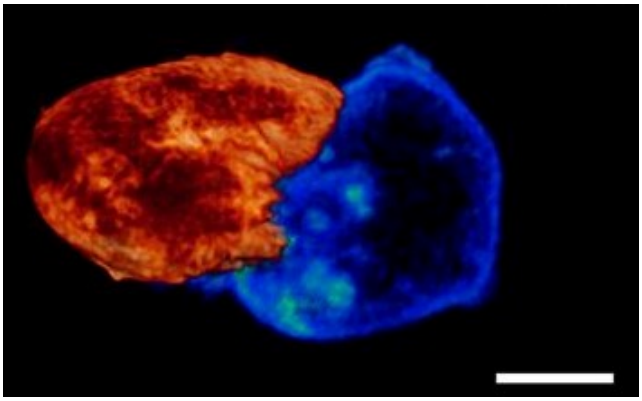

Figure 1.3.: Two-color volume rendering interaction of a T cell (orange) with a target cell (blue) after immunological synapse formation. Image taken from [8]. The scale bar corresponds to 5 µm.

1.3. Model system for antigen presenting cells

To enable the study of the TCR and pMHC, in this thesis the antigen presenting cell is replaced by a two-dimensional functionalized supported lipid bilayer for easier examining under the microscope.

The region of the T cell in direct and stable contact with the antigen presenting cell is called the immune synapse. Because the immunological synapse is formed between two cell membranes in 3D space, it is hard to observe the synapse directly under a fluorescence microscope. Using a supported lipid bilayer as a model for the antigen presenting cell has the advantage of all synapses forming in the same plane, which can be easily focused on with the microscope, compared to close contact of two cell membranes in 3D space. Additionally, the close proximity to the glass slide allows the use of Total Internal Reflection Fluorescence microscopy (see subsection 1.4.3) to achieve a high contrast by suppressing out-of-focus light.

Further, as explained in subsection 1.1.2, there are many kinds of T cells in the body, each expressing a different T cell receptor unique for its antigen. The 5cc7 mouse line was used in this thesis, which has an altered immune system to only produce $CD4^+$ T cells specific for the peptide called *moth cytochrome C (MCC)*. Using 5cc7 derived T cells in conjunction with the correct pMHC, the interaction of the specific pMHC together with the TCR can be observed.

1.3.1. Supported lipid bilayers

A supported lipid bilayer is formed by putting a solution of lipid vesicles onto a hydrophilic glass surface, where they burst open.

The polar heads of the lipids face the water outside the bilayer, while the hydrophobic tails point inwards. See Figure 1.5 for an illustration. Because the bilayer has a thickness of approximately 5 nm but can be spread over several millimeters it can be considered an almost perfect two dimensional material.

By using similar lipids as in the cell membrane and by attaching proteins to the bilayer, model systems for cell membranes can be formed to be studied in reproducible conditions.

98 % DOPC and 2 % DOGS-NTA-Ni, a synthetic diacyl lipid with a His-tag binding head group, are used to form the bilayer. The membrane proteins Intercellular Adhesion Molecule 1 (ICAM-1) and pMHC are attached via His-tags. ICAM, expressed on antigen presenting cells, plays an important

role by binding to integrins of the T cell and mechanically strengthening the synapse. This forms a simplified model of the antigen presenting cell seen in Figure 1.3. DOPC is a glycerophospholipid, which is found in cell membranes (see Figure 1.4 for its structure). Its polar head consists of phosphatidylcholine connected to the sn3 end of glycerol. The sn1 and sn2 ends of the glycerol are connected to oleic acids, which form the hydrophobic tail. Due to them being unsaturated they have a low melting temperature. DOPC melts at a temperature of $-17\,^{\circ}\mathrm{C}$ and is therefore in liquid phase at room temperature [9]. As a result attached proteins diffuse freely.

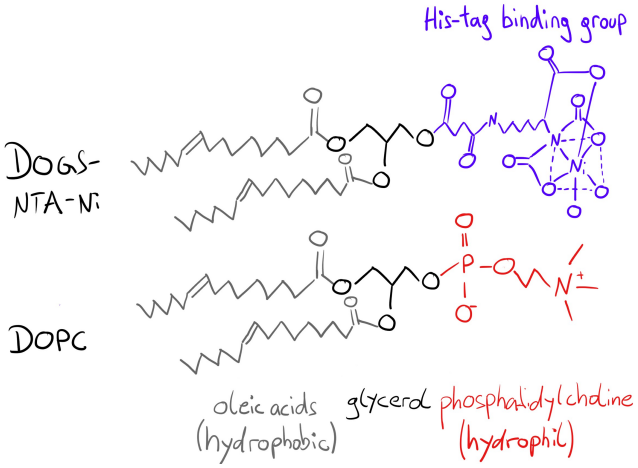

Figure 1.4.: Structure of 1,2-dioleoyl-sn-glycero-3-[(N-(5-amino-1-carboxypentyl)iminodiacetic acid))succinyl] (DOGS-NTA-Ni) and 1,2-dioleoyl-sn-glycero-3-phosphocholine (DOPC).

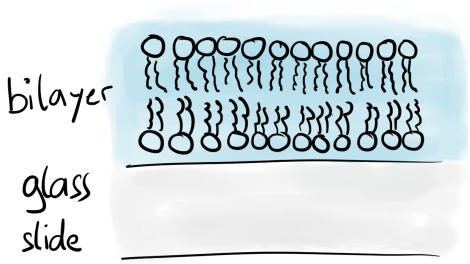

Figure 1.5.: Illustration of a planar lipid bilayer supported on a glass slide. The polar heads of the lipids point outward, while the hydrophobic tails point inward to minimize contact with the polar water molecules.

1.4. Microscopy

1.4.1. Fluorescence microscopy

A fluorescence microscope can be to study the interaction of fluorescently labelled single molecules. Usually in biology a low contrast sample is stained with fluorophores to add contrast. In fluorescence microscopy, photons, for example provided by a laser, excite the fluorophores, which in turn emit light themselves. This emission forms an image and is recorded.

Fluorophores can be selectively excited by a high energy photon and emit a lower energy photon in return. As they absorb a photon, an electron in the ground state gains energy and moves to a higher state. There it might relax, without emitting a photon, through vibrational or rotational states, but still remain in an excited state. From this state it can relax to the ground state by emission of a lower energy photon. See Figure 1.6 for an energy diagram called the Jablonsky diagram of a fluorophore.

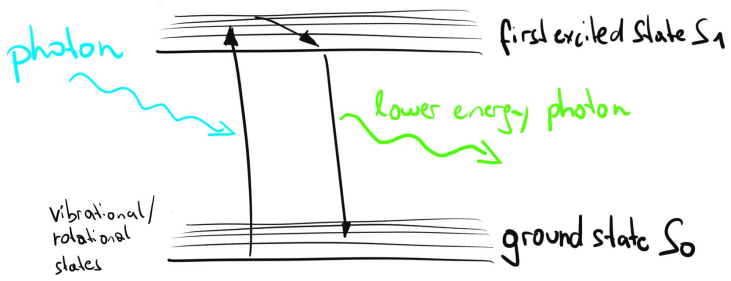

Figure 1.6.: Illustration of a Jablonsky diagram of a fluorophore excitation and emission.

Fluorophores have characteristic excitation and emission spectra, with the emission maximum shifted to lower energies, called Stokes shift. See Figure 1.13 for a fluorescence spectrum of a fluorophore.

Because the intensity of emitted light is much lower than the excitation light, the excitation light needs to be filtered to form a usable image. Here the Stokes shift is important, because the lower wavelength excitation light can be filtered due to its spectral distance from the emission light. The key component is the dichroic mirror, which can selectively reflect or transmit

light below or above a certain wavelength. Such a mirror can be chosen to fit the fluorophore.

To filter out photons with undesirable wavelength in the excitation beam path, an excitation filter is placed before the light hits the sample. The excitation light gets reflected by a dichroic mirror into the objective, leading to the illumination of the sample.

The fluorescence emission produced by the sample gets collected by the objective and is transmitted by the dichroic mirror and focused by the tube lens to form an image on the chip of an EMCCD camera. Because the dichroic mirror is not perfect, it does not separate the high power excitation light from the low power emission light completely. Therefore, an emission filter is placed in the beam path after the dichroic mirror. See Figure 1.7 for the optical path of a fluorescence microscope.

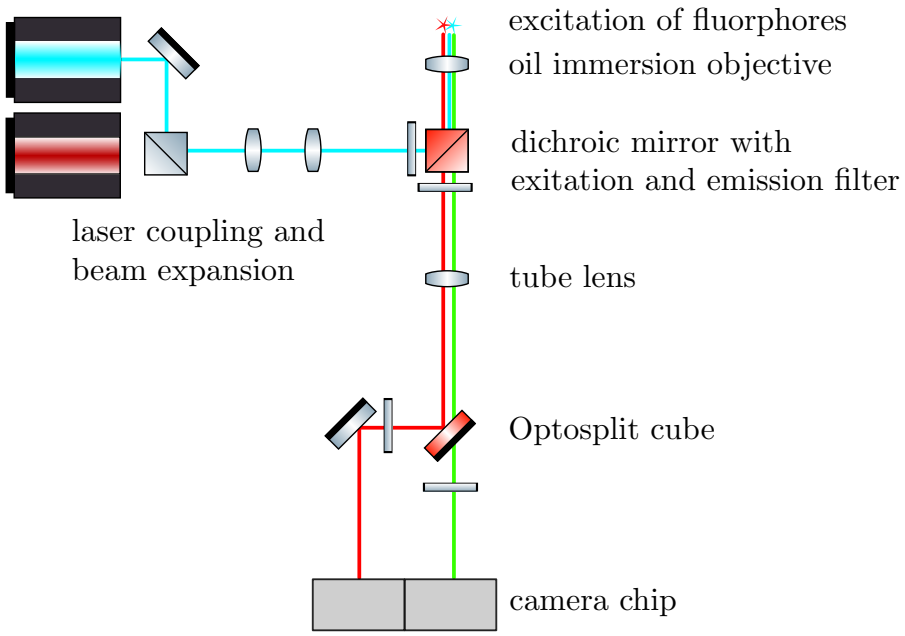

Figure 1.7.: Basic representation of the optical path of a fluorescence microscope. The laser gets reflected via a dichroic mirror and passes through the objective upon the sample, where it excites the fluorophores. Emission light passes through the objective and dichroic mirror to form an image on the camera chip. The optosplit with another dichroic mirror splits apart the two colour emission spatially in the image.

If the sample emits in two colours (like in subsection 1.4.4), they both pass the dichroic mirror and emission filter, but get separated into two images by an optosplit cube. Inside the optosplit cube are a dichroic mirror to split both colours and further filters to compensate for the imperfect dichroic mirror.

1.4.2. Single molecule microscopy

When imaging the light coming from a single molecule, one has to keep in mind that these, similar to point light sources, appear as extended disks due to diffraction. In this section the physical limit of resolution in a microscope is discussed to understand the restrictions of single molecule microscopy.

The infinity corrected microscope places the sample in the focus of the objective, so each light point source in the sample plane leaves the objective as a parallel wave. Therefore, the image distance of the objective is at infinity. The tube lens, positioned at any distance from the objective, forms an image at its back focal plane, where a camera is located. See Figure 1.9 for a simplified beam path.

Parallel light passing through a round aperture with radius R[1] and focused with a lens with focal length f_2 forms a diffraction limited spot, called the Airy disk, with the distance p of its first minimum at

$$p = 1.22\frac{f_2\lambda}{2R} \tag{1.1}$$

and λ the wavelength of the light [10]. See Figure 1.8 for the beam path producing the airy disk.

Inserting the magnification of a microscope $M = -\frac{f_2}{f_1}$, where f_1 in the focal length of the objective and f_2 the focal length of the tube lens, into Equation 1.1 leads us to the modified form:

$$p = 1.22\frac{Mf_1\lambda}{2R}. \tag{1.2}$$

[1] Usually the limited size of an objective already acts an aperture.

R can be written as $R = f_1 \tan\vartheta$, with ϑ the maximal half-angle of the cone of light that can enter or exit the lens (see Figure 1.9). Using the paraxial approximation for $\vartheta << 1$, R can be written as $R = f_1 \sin\vartheta$ or

$$R = f_1 \mathrm{NA} \tag{1.3}$$

using $\mathrm{NA} = n \sin\vartheta$ for a refraction index $n = 1$ for air.

Inserting Equation 1.3 into Equation 1.2 leads to $p = 1.22\frac{M\lambda}{2\mathrm{NA}}$ or with d, which corresponds to p but in object space, to the famous equation for a diffraction limited spot:

$$d = 1.22\frac{\lambda}{2\mathrm{NA}} \tag{1.4}$$

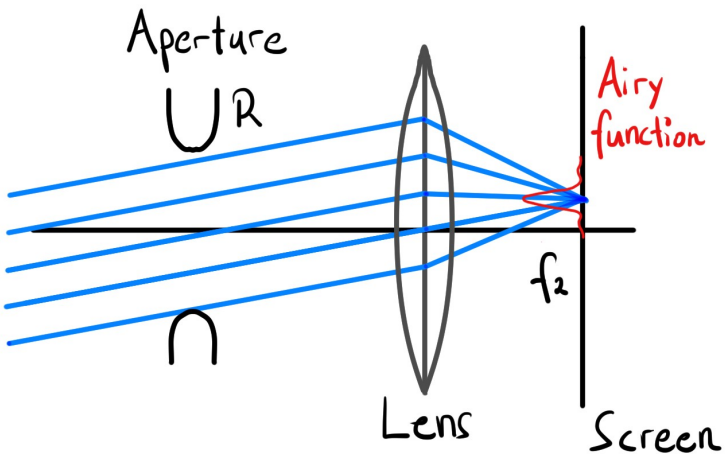

Figure 1.8.: Parallel beams passing through an aperture with radius R to form an image after the lens at the focal point f_2, the so-called Airy function.

The size of a diffraction limited spot can be calculated with Equation 1.4 and is approximately 200 to 300 nm for wavelengths of 488 to 640 nm and a numerical aperture of 1.33 (for water). The size of the proteins to be observed are below 10 nm, so they cannot be observed individually if the distance between them is below the size of a diffraction limited spot.

Although not very bright, single molecules can be observed by using sensitive cameras and making sure the distance between fluorophores is larger than the size of an airy disk. An electron-multiplying charged coupled device

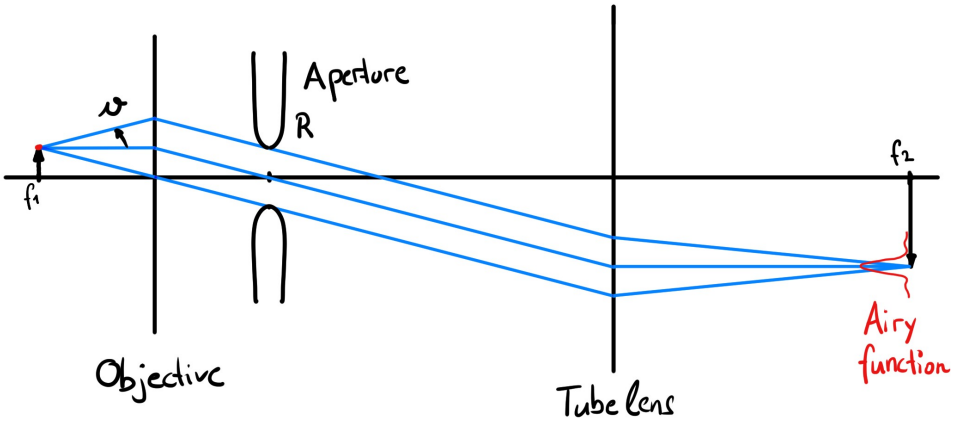

Figure 1.9.: Simplified beam path of an infinity corrected microscope. The light in the focus of the objective leaves the objective in the form of parallel waves. The aperture with size R limits the angles of light accepted by the objective and defines the accepting angle ϑ. The tube lens forms the parallel light into an image of the object on the screen.

(EMCCD) camera, which amplifies electrons produced by photons directly on the chip, was used in this thesis to sensitively detect low light of the fluorophores. Further, Total Internal Reflection Fluorescence (see subsection 1.4.3) was used to excite only the fluorophores of interest.

1.4.3. Total Internal Reflection Fluorescence (TIRF)

Since the fluorophores of interest were in the bilayer and on the opposing cell membrane, both close to the glass slide, Total Internal Reflection Fluorescence (TIRF) Microscopy was used to help reduce interfering signals from other fluorophores.

To achieve TIRF, the angle of parallel beams of the excitation light is tilted until there is total reflection on the boundary between glass and the imaging buffer. Due to the total reflection the laser does not pass into the imaging buffer, except for an evanescent wave, which excites fluorophores that are in an approximate 200 nm region above the glass slide. See Figure 1.10 for a basic diagram of TIRF.

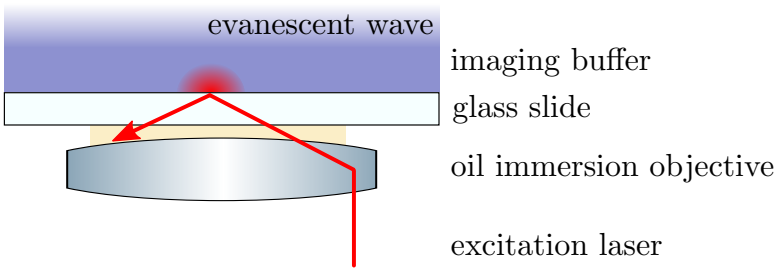

Figure 1.10.: Basic representation of a Total Internal Reflection Fluorescence microscope. The laser focused off-center at the back focal plane of the objective leaves it as parallel tilted wave to hit the glass slide and image buffer boundary forming a total reflection. The evanescent wave excites only fluorophores close to the glass slide.

The laser is focused on the back focal plane of the objective. By definition all beams focused in the back focal plane leave the objective as parallel beams. By moving the focused spot away from the optical axis, the parallel beams will tilt. The farther off center the spot is, the larger the angle becomes. See Figure 1.11 for a sketch of TIRF.

1.4.4. Förster Resonant Energy Transfer (FRET)

An effect called Förster Resonant Energy Transfer (FRET) was used in Huppa et al. [1] and in this thesis to observe binding events between the T cell receptor and peptide MHC.

FRET is a non-radiative energy transfer occurring between a donor and acceptor fluorophore that are in close proximity of each other. After excitation of the donor by a high energy photon, it transfers the energy to a acceptor, which emits a lower energy photon. The efficiency of the energy transfer E depends on the distance R according to

$$E = \frac{1}{1 + (R/R_0)^6}, \tag{1.5}$$

where R_0 (the so-called *Förster radius*) is a constant representing the distance where 50 % of the energy is transfered [12]. R_0 is typically around 3 to 7 nm and depends on the refractive index n, the quantum donor yield Q_D, the

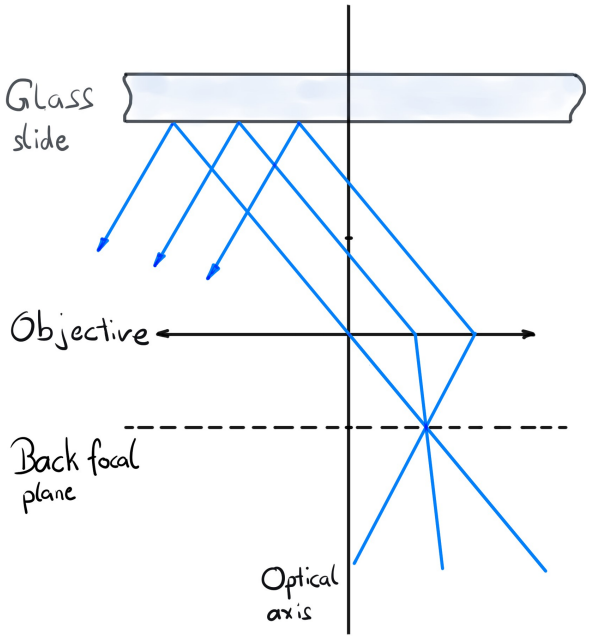

Figure 1.11.: Beam path of the laser in TIRF. The parallel beams' angle with respect to the optical axis increases the further the laser is focused off the optical axis in the back focal plane of the objective. If the angle is large enough, the parallel beams undergo total reflection on the glass boundary.

relative mutual orientation of donor and acceptor dipoles κ^2 and the overlap integral of donor and acceptor spectra $J(\lambda)$ according to

$$R_0^6 \simeq \kappa^2 Q_D n^{-4} J(\lambda). \tag{1.6}$$

Usually a value of 2/3 is used for κ^2, which is the average of all possible mutual orientations [11]. The spectra of donor and acceptor can be seen in Figure 1.13.

See Figure 1.12 for illustration of FRET. Due to the strong $\propto R^6$ dependence on the distance between the donor and acceptor fluorophores, the FRET efficiency can be used as read-out for molecular interactions.

In the case of this thesis, donor fluorophore labelled T cell receptors and acceptor fluorophore labelled pMHC ligands were used to study their binding and unbinding behaviour.

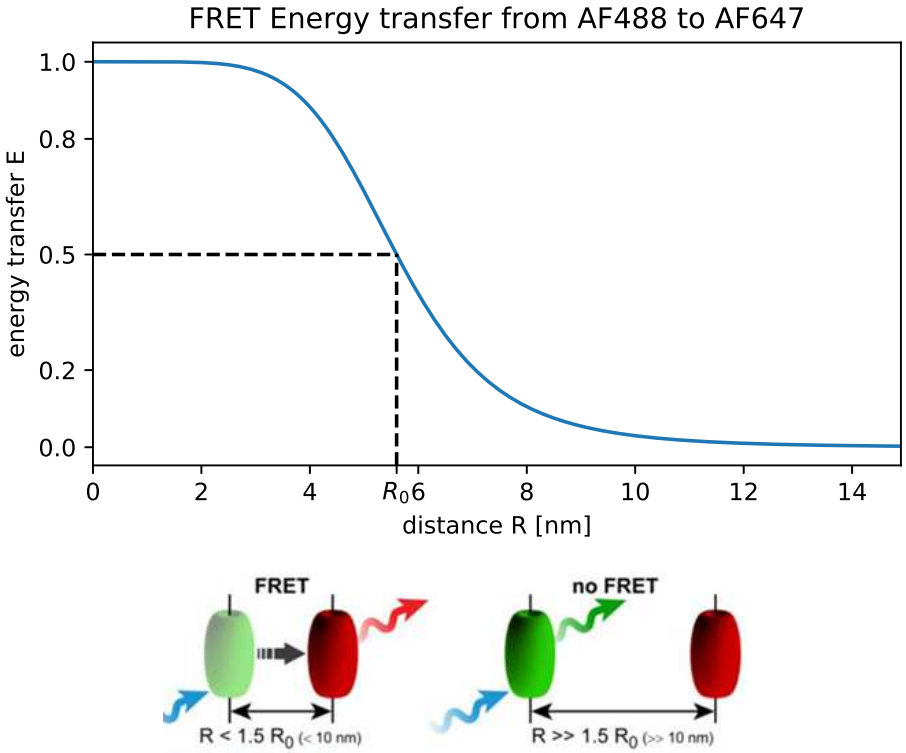

Figure 1.12.: **Top:** Plot FRET efficiency E depending on the distance between the fluorophores AF488 to AF647 (see Equation 1.5). The Förster radius $R_0 = 5.6\,\text{nm}$ is indicated by the dashed line. **Bottom:** FRET transfers energy from the donor to the acceptor fluorophore if the distance between them is smaller or larger than approximately $1.5R_0$. Image taken from [11].

Donor bleed-through and cross excitation

The acceptor channel contains not only the actual FRET emission, but also other unwanted contributions. This includes the so-called cross excitation, which is the light emitted by the acceptor due to direct excitation by the donor excitation laser. This happens because the excitation spectrum of the acceptor is nonzero at the donor laser wavelength.

Furthermore, the so-called bleed-through consists of donor emission light, which penetrates spectrally into the acceptor channel, since the donor emission spectrum is nonzero at the wavelength range transmitted by the acceptor

channel filters.

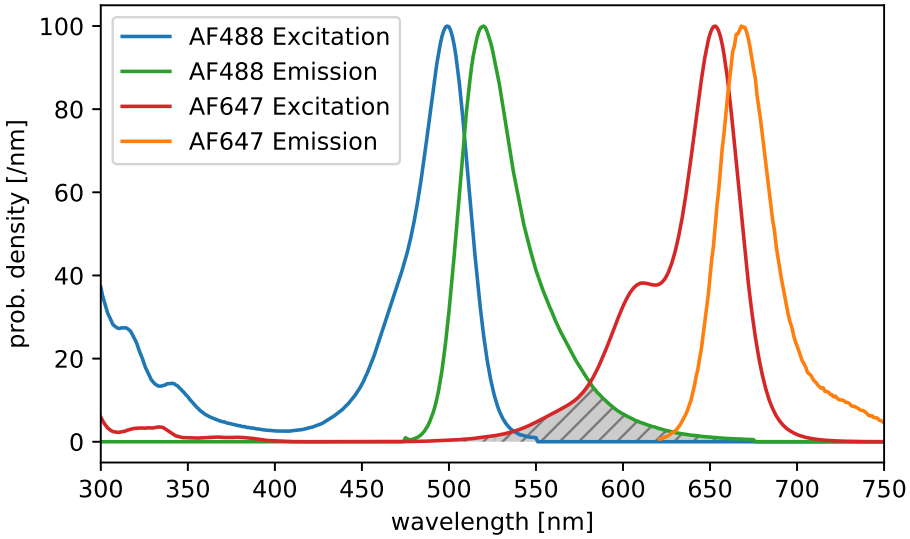

Figure 1.13.: Excitation and emission spectra for the donor AF488 and acceptor AF647 FRET pair. The stokes shift of the peaks from higher energy excitation spectrum to lower energy emission spectrum can be seen. The gray hatching shows where the emission spectrum of AF488 overlaps with the excitation spectrum of AF647 (see the overlap integral $J(\lambda)$ of Equation 1.6).

1.5. Previous studies measuring binding kinetics

Both Huppa et al. [1] and O'Donoghue et al. [2] model the immunological synapse by placing 5cc7 T cells on a mobile supported lipid bilayer decorated with pMHC and murine Intercellular Adhesion Molecule (mICAM). mICAM is an adhesion protein and helps T cells adhere to the bilayer. The cells spread on the bilayer, forming a synapse which can be observed by fluorescence microscopy. Using the correct, in this case the *moth cytochrome C (MCC)*, peptide sequence in the pMHC, the T cells activate depending on the concentration of pMHC on the bilayer. If a different peptide sequence is used, the T cells do not activate. See Figure 1.14 for an illustration of both models.

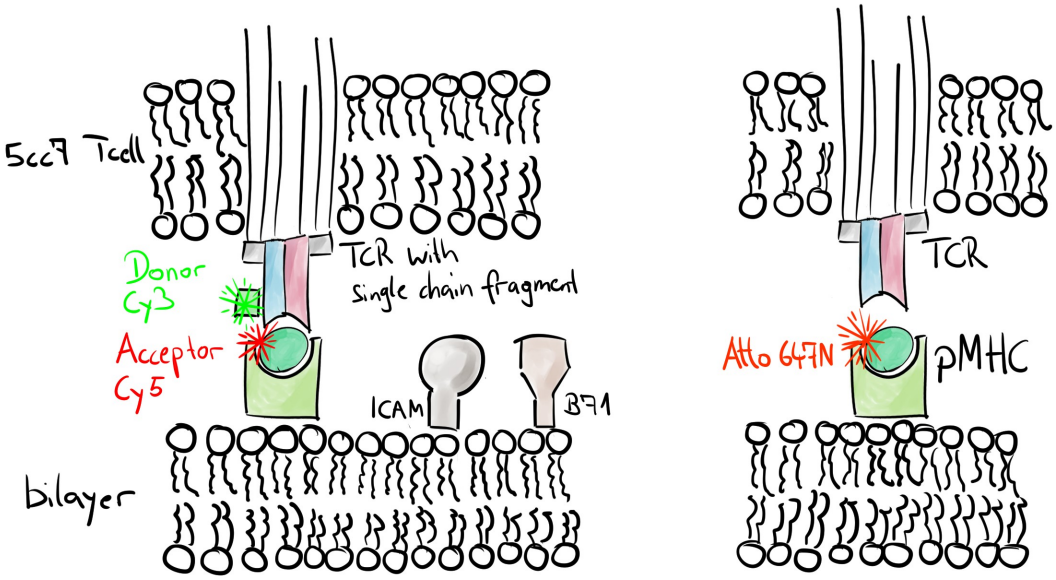

Figure 1.14.: Model of immunological synapse using a bilayer with labelled pMHC and ICAM as the antigen presenting cell. **Left:** Huppa et al. [1] labelled the T cell receptor with a single chain fragment to measure binding with FRET. **Right:** O'Donoghue et al. [2] did not label the TCR, but inferred binding kinetics from immobilization durations employing long exposure times.

Huppa et al. [1] labelled both the TCR and the pMHC and used FRET, which is highly distance dependent, to observe binding events directly. Only the specific event of TCR and pMHC binding led to FRET, which could be observed and used to calculate the binding dynamics.

They used a single-chain variable fragment (scFv) derived from H57, an antibody against TCR. It was labelled with Cy3 as a FRET donor and bound to the T cell receptor (see Figure 1.15). Together with the Cy5 labelled MCC-pMHC it was used to measure the lifetime of FRET signals. For this Huppa et al. [1] used high abundance or bulk labelled T cell receptors and single molecules for the FRET acceptor pMHC. They managed to observe the localization of single appearing and disappearing FRET events and calculate the lifetime by correcting for photo bleaching. Huppa et al. [1] measured off-times τ_{off} of approximately 100 ms at 37 °C. FRET signals were highly specific and were only observed using the MCC-pMHC.

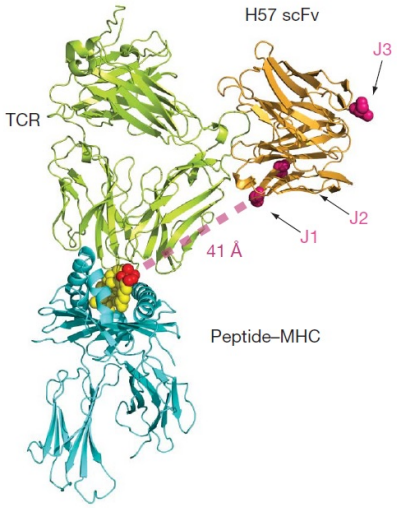

Figure 1.15.: Composite model of H57 derived single-chain variable fragment (scFv) used by Huppa et al. [1] bound to the T cell receptor and in contact with pMHC. J1 to J3 indicate dye attachment sites with varying distance. Image taken from [1].

O'Donoghue et al. [2] used a ATT647N-labelled MCC-pMHC, which was mobile and diffused on the bilayer based on Brownian motion. Using an exposure time of 17.5 ms they resolved single molecules of pMHC over hundreds of frames with high mobility. With the addition of T cells due to the pMHC interaction with the TCR, some pMHC became immobilized.

By using long exposure times of 500 ms combined with low laser power of $0.02\,\mathrm{W\,cm^{-2}}$, all more rapidly diffusing pMHC formed a blurred background, while slow moving molecules remained highly localized and therefore indicated a binding event. These slow moving localizations only appeared using the activating pMHC and were used to derive binding times of approximately 5 s.

2. Materials and methods

2.1. Lipid bilayer

For the preparation of the test chambers, Menzel Deckgläser #1.5 coverslips were plasma cleaned and glued onto clean Lab-Tek chambers with Picodent Twinsil silicon. The plasma cleaning leads to the glass slide being hydrophilic, which aids the formation of the bilayer.

Small unilamellar lipid vesicles were produced by sonification of lipids suspended in 10x phosphate buffered saline (PBS). The lipid mixture consisted of 98 % 1,2-dioleoyl-sn-glycero-3-phosphocholine (DOPC) and 2 % 1,2-dioleoyl-sn-glycero-3-[(N-(5-amino-1-carboxypentyl)iminodiacetic acid)succinyl] (Ni-NTA-DOGS). The vesicles were pipetted onto the glass surface and incubated, where they burst and formed the bilayer for 20 min. After that, using 1x PBS the remaining vesicles were burst and washed away.

In each chamber, 5 pg of His-tagged pMHC and 32 ng of His-tagged mouse ICAM (mICAM) were added and after 75 min incubation time, excess protein was washed off with PBS again.

The bilayers were always prepared on the day of the experiment with vesicles not older than five days.

2.2. T cells

To prepare 5cc7 T cells for the experiments, they were centrifuged and pelleted in Hanks Buffered Salt Solution (HBSS). The excess HBSS was removed and a concentrated cell suspension remained.

23 ng of AF488-labelled H57 derived single chain fragment (scFv) was added to the T cells and incubated for 20 min on ice.

The unbound scFv was washed off by diluting the cell suspension with HBSS and then centrifuging and removing supernatent HBSS again. The cells were stored on ice until used for the experiments.

All centrifugation was done at 22 °C and an RCF of 350 for 3 min (Program 1 at the time of writing this thesis).

2.3. Microscopy

The PBS in the test chamber was exchanged for HBSS (Hanks Buffered Salt Solution) as an imaging buffer and then the T cells were pipetted into the test chamber.

The bilayer and T cells were imaged by an inverted fluorescence microscope (Zeiss Axiovert 200) with an oil objective (ZEISS α Plan APOCHROMAT 100x/1.46 Oil DIC (UV) VIS-IR). The fluorophores were excited either with red (640 nm) or blue (488 nm) lasers by reflecting them into the sample trough the dichroic mirror (cutoff wavelength at 640nm) and emission filter (ZET488/640m-TIRF) under an angle appropriate for TIRF. Light emitted from the fluorophores passes through the dichroic mirror and 1x tubelens into the Optosplit.

The Optosplit cube spatially separates the light according to wavelength and projects two images onto the camera sensor. This is done using another dichroic mirror (cutoff wavelength of 640 nm) and filters for each image (675/50 nm and 525/45 nm respectively).

Because the blue image would saturate the camera due to high fluorophore density on the T cells, an additional optical density filter (OD 0.5) was used in the blue emission channel. A correction lens (IO115) was inserted into the red beam path to correct for longitudinal chromatic aberration and have both the blue and the red channel in the same focal plane. Both images then form on a electron-multiplying CCD camera (Andor iXon 897 Ultra camera).

The camera was set to a pre amp gain of 1, an EM gain of 300 and horizontal shift frequency of 17 MHz.

See Figure 1.7 for a diagram of the simplified optical path and Figure 2.1 for the illumination protocol.

Additionally, because two color images were acquired, fluorescent TetraSpeck beads were imaged to be able to overlay color channels and correct for lateral chromatic aberrations (see section 2.4).

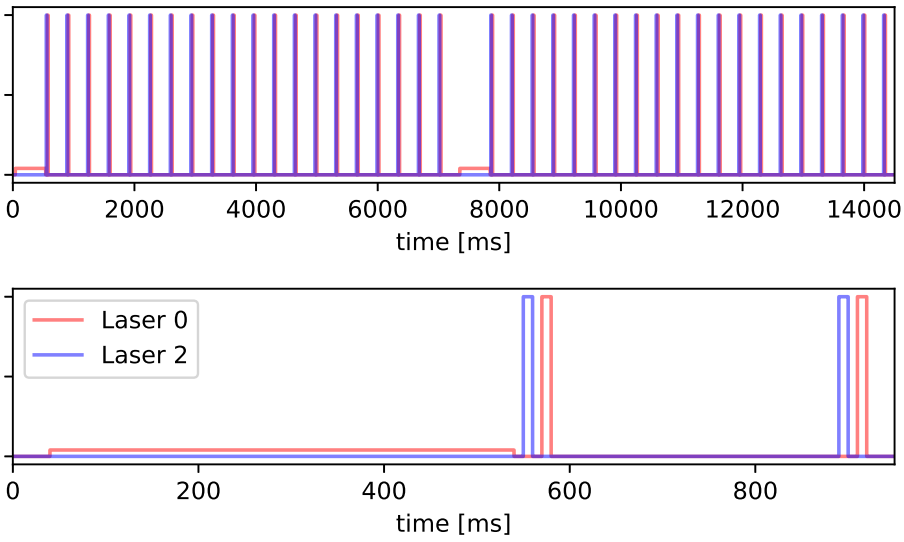

Figure 2.1.: **Top:** Plot of the illumination sequence used for the experiments. A combination of single 500 ms acceptor excitation image followed by twenty 10 ms donor and acceptor excitation images were taken and the repeated once. The delay between the images was 10 ms and 300 ms. **Bottom:** Zoom of the first few excitation sequences from above.

2.4. Data analysis

The data was analyzed using the *sdt* Python package (version 13.4) and the *Jupyter notebook* [13].

Fluorescent beads were localized in two-color images by means of the 3D-DAOSTORM algorithm [14]. Since each bead is visible in both color channels, this can be used to calculate the transformation function for coordinates in one channel to coordinates in the other channel.

Using the 3D-DAOSTORM algorithm the pMHC in the acceptor channel was localized in all types of illumination: acceptor excitation with long and short exposure times, and donor excitation (for details see section 3.1 and section 3.2). The localizations found by the 3D-DAOSTORM algorithm were linked between frames to form trajectories using the *trackpy* Python package [15].

The transformation function acquired from fluorescent bead data was used to convert the position of the localizations in the acceptor image to positions in the donor image.

An interactive *Jupyter widget* (see Appendix A) was written to visualize and explore the image data in the context of FRET analysis. The widget shows both the donor and acceptor channel images with adjustable contrast at the same time. Both the image data set (cell number) and frame can be interactively chosen and previously found localizations and trajectories displayed. The positions on the donor image were marked and enabled the differentiation between bleed through and possible FRET events.

3. Results

A DOPC bilayer containing ICAM and AF647-labelled pMHC was used as a model of the immunological synapse. T cells with its T cell receptors labelled with AF488 scFv were seeded onto the bilayer. The illustration of the synapse can be seen in Figure 3.1.

This model is similar to Huppa et al. [1], but differs in two aspects. First the dyes were changed to AF488 and AF647 as modern replacements for Cy3 and Cy5, with only a small difference in Förster radius R_0 of 6 nm [16] compared to 5.6 nm of AF488–AF647. Secondly B7 was omitted because it was not available at the time of the experiments.

The system is also essentially the same as in O'Donoghue et al. [2], apart from the TCR not being labelled for the long exposure measurements and the use of AF647 instead of Atto 647N on the pMHC.

3.1. Long exposure times

AF647-labelled MCC pMHC in single molecule density together with ICAM was observed on the bilayer system. With short exposure times, single molecules were visible as clearly defined features while diffusing due to Brownian motion and could be localized by 3D-DAOSTORM (see section 2.4). Using long exposure times of 500 ms the diffusing signals were spread over many pixels and formed blurred trajectories, which could not be localized. Only pMHC which is immobile on time scales of 500 ms would be detectable with clear localizable features.

Upon the addition of MCC pMHC selective T cells to the bilayer, the MCC pMHC bind to the TCR and became immobilized in the immunological

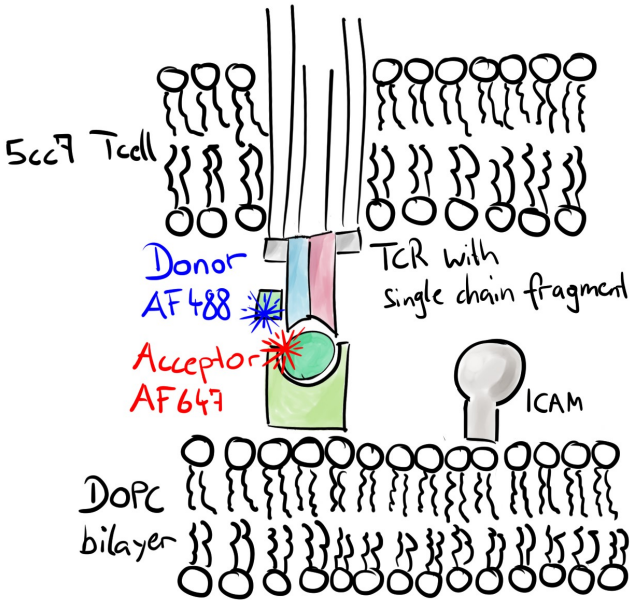

Figure 3.1.: Model of the immunological synapse used for FRET and long exposure time measurements. It is very similar to Huppa et al. [1], except for a lack of B7 protein in the bilayer, AF488 instead of Cy3 as FRET donor and AF647 instead of Cy5 as acceptor.

synapse. These immobilized pMHCs could be easily distinguished from the mobile ones due to their well-defined features in long exposure time images and occurred only under the cell, where the immunological synapse was. This is in good agreement with O'Donoghue et al. [2] and can be seen in Figure 3.2.

To check if the immobilizations are specific to the 5cc7 TCR and MCC pMHC interaction, a class I pMHC (H-2K^b) which cannot interact with the 5cc7 mouse TCR was used. H-2K^b was often immobilized even before the addition of T cells. However, adding T cells did not increase the number of H-2K^b pMHC immobilizations (data not shown). This indeed indicates specificity.

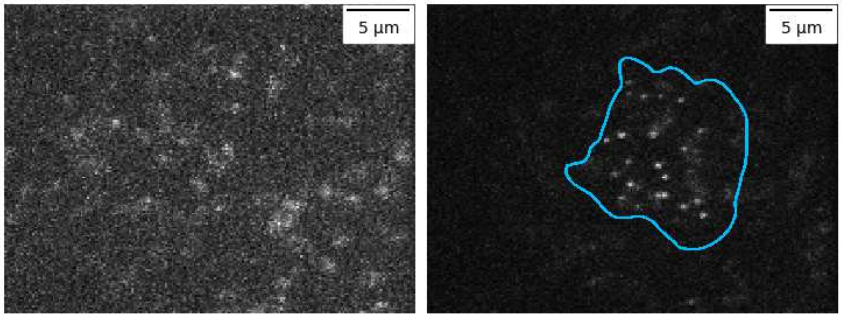

Figure 3.2.: **Left:** Long exposure image of a bilayer containing Alexa 647-labelled MCC pMHC. The pMHC is mobile and completely blurred due to diffusion during 500 ms exposures. **Right:** Same bilayer after addition of T cells selective to MCC pMHC. The T cell is indicated by a blue border. Binding to T cell receptors immobilizes pMHCs, which are clearly visible as distinct bright spots. pMHC that is unbound, in particular next to the cell, did not show these features.

3.2. Combination with FRET

T cells with AF488-labelled scFvs were put on a bilayer with single molecule density of AF647-labelled pMHCs. By saturating TCRs with scFvs, the likelihood of FRET events was maximized.

To be able to observe FRET, the donor had to be excited with a laser power suitable for single molecules. However, this led to high intensity fluorescence due to the high fluorophore density on the cells, saturating the camera pixels. A suitable optical density filter was therefore put into the blue emission beam path.

To find the appropriate intensity of the blue laser, scFv bulk labelled cells were photobleached until no fluorophore was left in the immunological synapse. Afterwards single molecules of labelled TCR diffused along the membrane into the synapse and could be imaged. The blue laser power was adjusted to yield sufficient signal to noise ratio of the FRET signal assuming a FRET efficiency of 10 to 20 %.

Originally Fetal Calf Serum (FCS) was added to the HBSS imaging buffer, but it this caused high amounts of red fluorescence, making it difficult to

distinguish single fluorophores or later FRET signal from background. As no other solution could be found, it was simply omitted. See Figure 3.3 for the comparison between a bilayer with and without FCS in the imaging buffer.

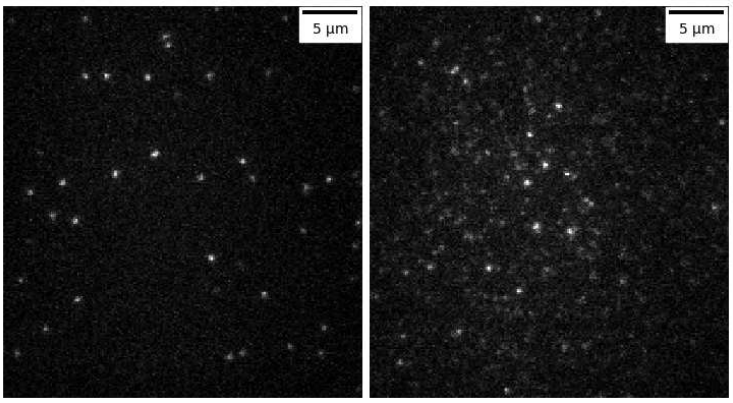

Figure 3.3.: **Left**: AF647-labelled pMHC on a DOPC bilayer with HBSS (Hanks Buffered Salt Solution) as imaging buffer. **Right**: AF647-labelled pMHC on a DOPC bilayer with HBSS 98 % + 2 % FCS (Fetal Calf Serum) as imaging buffer. Notice increased background in the right image.

To avoid photobleaching, cells were found using the transmission light and the microscope was focused on the immunological synapse using the lowest possible red laser intensity.

An illumination protocol was designed to localize bound pMHC with long exposure times and examine possible FRET events of the immobilized pMHC with short exposures. First, like in section 3.1, a 500 ms long exposure time image was taken at acceptor excitation. Then a series of short exposure time (10 ms) images with alternating donor or acceptor excitation was acquired (see Figure 2.1). The same illumination protocol was used for all measurements described in this section.

To be able to observe any FRET-like events (see Figure 3.4), TIRF had to be optimized for the donor excitation, even though this led to worse signals during acceptor excitation.

Many events in the acceptor channel upon donor excitation have corresponding localizations of acceptor pMHC in either the long or short exposure acceptor excitation image, indicating FRET events. Some of these events may be

caused by high amounts of donor bleed through due to local TCR enrichment and would have to be filtered out.

Most FRET-like events disappear or bleach after one frame. In later frames only few new FRET events appear (data not shown).

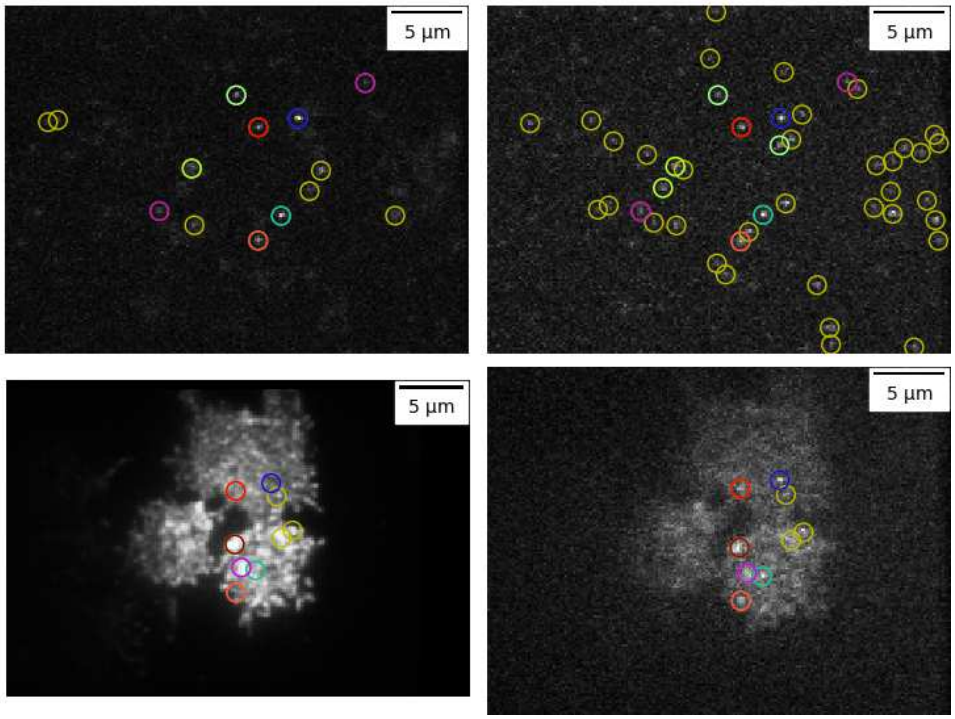

Figure 3.4.: **FRET sequence** images of AF488 scFv labelled T cells on a bilayer containing MCC pMHC labelled with AF647. The differently colored circles correspond to localized fluorophores that could be tracked through time and yellow circles indicate fluorophores localized in a single image only. **Top Left**: Long exposure acceptor excitation image showing the immobilizations of the pMHC. **Top Right:** Short acceptor exposure image. Additionally, mobile pMHC, which are not bound to a T cell receptor, are visible. Since the image was taken after the FRET excitation, some fluorophores were already bleached. **Bottom Left:** The donor channel upon donor excitation shows T cell receptors forming the immunological synapses. **Bottom Right:** Image of the acceptor channel upon donor excitation. Some of the FRET-like events (e.g. dark blue, orange and red) can also be seen during acceptor excitation and are not exceptionally bright in the donor image, which indicates proper FRET events. Others (e.g. dark red) are likely caused by bleed through of the bright spots in the donor image.

3.2.1. Control experiments

All control experiments were designed so that there is no FRET possible, by either having no acceptor or no donor for FRET. Nevertheless, FRET-like events could be observed.

The control seen in Figure 3.5 used unlabelled T cells on a bilayer with AF647-labelled pMHC. Illuminating with the donor laser leads to mostly empty acceptor channels, except for some autofluorescence caused by the bright laser visible in both channels. Some localizations are visible in the acceptor channel while exciting with the donor laser and appear as FRET events. They cannot be explained by bleed through, because there is no bright feature in the donor channel.

Using non-fluorescent pMHC and the AF488-labelled scFv on the T cell receptor results in mostly blank images in the acceptor channel during donor excitation. Most localizations in the acceptor channel can be attributed to donor bleed through, but some localizations do not have a corresponding bright features in the donor channel and seem FRET-like (see Figure 3.6).

AF488-labelled cells on a glass slide with only HBSS, but no bilayer, are shown in Figure 3.7. The images show some autofluorescence of the cell during acceptor excitation. During donor excitation FRET-like events appear, some of which correspond to the localizations during acceptor excitation while others do not.

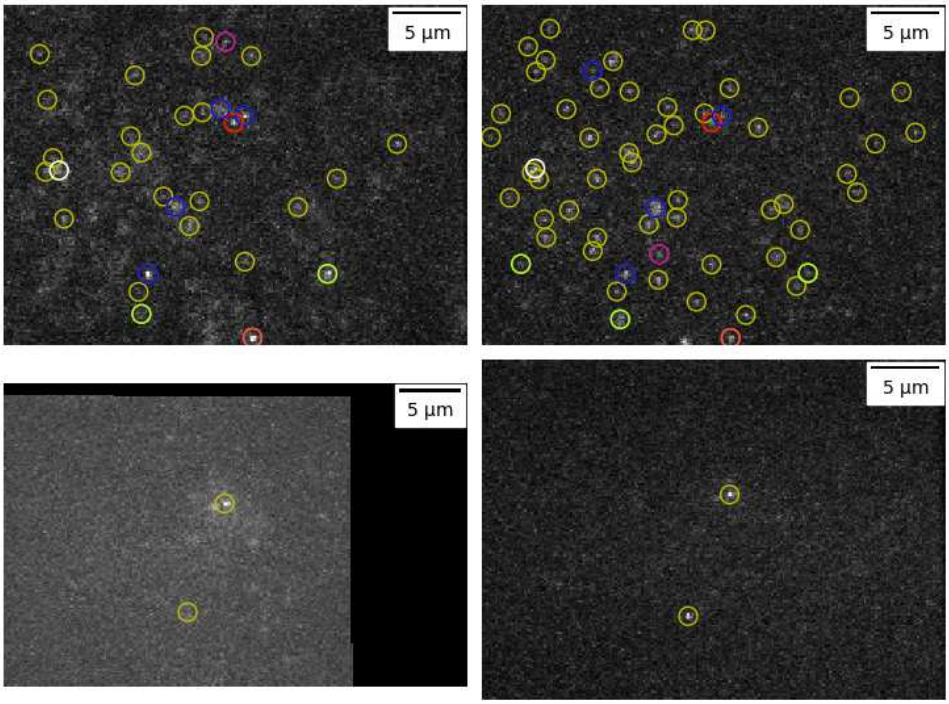

Figure 3.5.: **Control experiment** images of **unlabelled T cells** on a bilayer containing AF647-labelled MCC pMHC. Colored circles indicate localizations that were tracked through time, while yellow ones were localized only in a single image. **Top Left**: Long acceptor exposure image showing immobilizations due to the interaction of pMHC and T cell receptor as in Figure 3.4. **Top Right:** Short acceptor exposure image with additional mobile pMHC. **Bottom Left:** Image of the donor channel upon donor excitation showing localizations likely caused by autofluorescence of the T cells (not visible in the image, but found with transmission light). **Bottom Right:** Image of the acceptor channel upon donor excitation. Two localizations are indicated, but only the upper one co-localizes with the bright spot in the donor channel and can therefore be explained by autofluorescence or bleed-through.

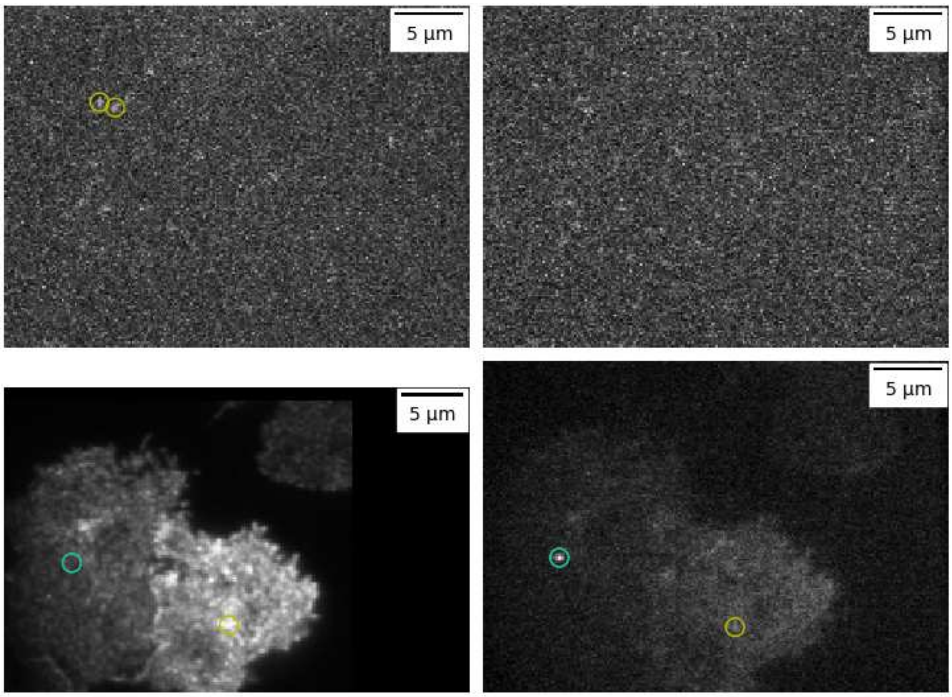

Figure 3.6.: **Control experiment** images of AF488-scFv labelled T cells on a **bilayer containing unlabelled MCC pMHC**. The circles indicate fluorophores localized by the 3D-DAOSTORM algorithm. **Top Left:** Long acceptor exposure image of bilayer with unlabelled pMHC. The marked signals might be attributed to noise due to permissive localization parameters. **Top Right:** Short exposure acceptor excitation. No fluorophores are visible. **Bottom Left:** Image of the donor channel upon donor excitation. AF488-labelled T cells forming the immunological synapse. **Bottom Right:** Image of the acceptor channel upon donor excitation. The localization indicated in yellow is likely due to bleed-through in contrast, the cyan localization appears FRET-like due to the low intensity at the corresponding donor channel position.

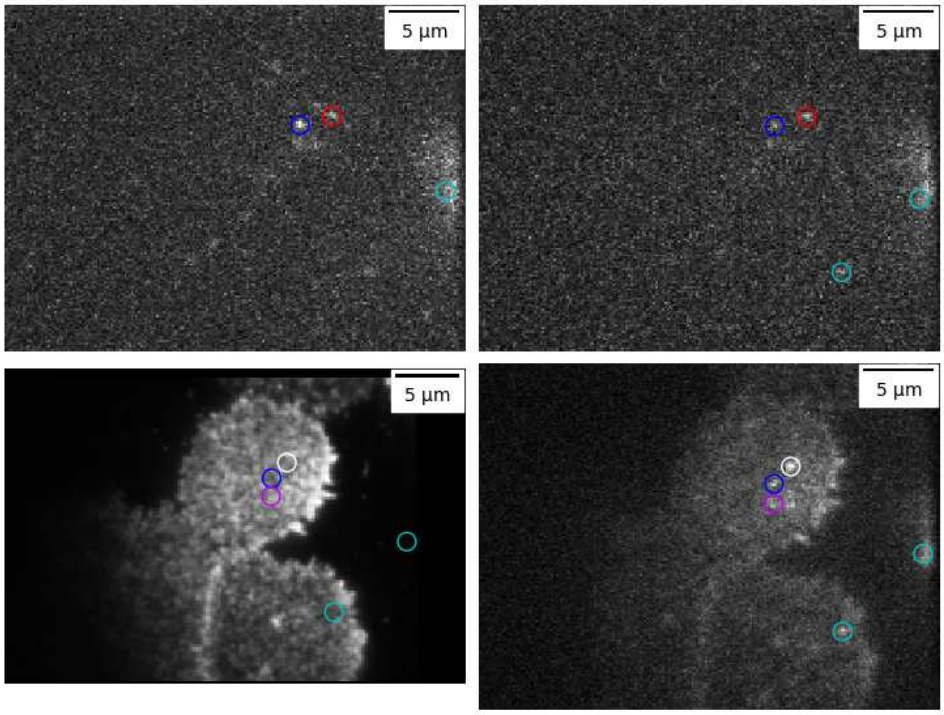

Figure 3.7.: **Control experiment** images of AF488 scFv labelled T cells on a **glass slide without a bilayer**. The circles indicate fluorophores localized by the 3D-DAOSTORM algorithm. **Top Left**: Long acceptor exposure image of T cells with donor fluorophore. **Top Right:** Short time acceptor excitation image. **Bottom Left:** Donor channel upon donor excitation of the AF488-labelled T cells forming the immunological synapse. **Bottom Right:** Image of the acceptor channel upon donor excitation. The white localization appears in the acceptor channel, but does not have any corresponding localization in the acceptor excitation images (top row). The blue localization has all the characteristics of a FRET signal even in the absence of an acceptor: It is visible in the acceptor channel and not exceptionally bright in the donor image.

4. Discussion

Most image series of the FRET measurements as well as the control images do not show FRET-like events (data not shown). The number of FRET-like events in the actual experiment seems to be higher compared to the controls, but for a proper statistical analysis many more experiments would have to be done to increase the sample size. Unfortunately there is no defining feature to filter out false positives. A common criterion is to select only localizations showing up in the acceptor channel but not in the donor channel, but these also occur in the control experiments.

Furthermore, the FRET-like events appearing in the first frame do not show up in later frames which indicates fast photobleaching. In later frames almost no new FRET-like events emerge. However, decreasing excitation laser power is not a viable option due to the signals already being weak.

If the FRET events in the experiments cannot be trusted, due to similar events in the control experiments, the question is: What causes these FRET-like events?

A possible explanation would be, that the AF488 scFv was contaminated with a FRET acceptor. In this case, images with only the AF488-labelled T cell and non-fluorescent pMHC (Figure 3.6) would show FRET due to that contamination. But then the FRET-like events should not appear in images where there is no AF488, as in Figure 3.5.

Another explanation could be that the cells' autofluorescence is causing FRET-like events. For example if some cellular feature could be excited with the red laser it could appear like a fluorophore during acceptor excitation. If the same feature could also be excited using the blue laser and its emission could be seen in both color channels, it could appear FRET-like, especially if the blue fluorescence cannot be discriminated from the bright background caused by the high density of AF488.

A solution could be to bleach the dense labels on the cells to almost single molecule levels or to dilute the scFv with unlabeled scFv. Because of the decreased noise caused by bleed-through, this might allow for better FRET signals to be seen in the acceptor channel. Further, some of the autofluorescence might also bleach and not recover, while fresh unbleached TCRs diffuse into the immunological synapse. However, with heavily labelled cells, there were already very few FRET events. In case of sparsely labelled TCRs, the number of events would drop even further due to the reduced likelihood of an unbleached TCR meeting a ligand.

There are some key differences in these experiments compared to Huppa et al. [1] that could have led to a different response of the T cells and therefore change the FRET results. The FCS in the imaging buffer was omitted due to red fluorescent contamination as discussed in section 3.2. Most importantly, experiments were performed under non-activating conditions, i.e., the pMHC density was much lower and the co-stimulatory protein B7 on the bilayer was left out. Huppa et al. [1] used a pMHC-Cy5 density of 30 molecules/μm^2, which is above the activation threshold, and bleached it down to single molecule level for the single molecule FRET measurements. Additionally, they employed a scFv-Cy3:TCR ratio of less than 1:6 to reduce bleed-through, improving the signal-to-noise ratio.

The possible solutions to address the problem of unspecific FRET-like events discussed above should be taken into consideration for future studies.

Appendix A.

Code for data analysis

On the following pages is the Python code of a Jupyter notebook used for the data analysis described in section 2.4.

[1]:
```
%matplotlib widget
import sdt.loc
import sdt.gui
import sdt.nbui
import sdt.chromatic
import sdt.io

import pims
import pandas as pd
import numpy as np
import matplotlib.pyplot as plt
import matplotlib.patches
plt.ioff()
from matplotlib_scalebar.scalebar import ScaleBar
import trackpy as tp
import glob

from scipy import signal
import random
from ipywidgets import interact, widgets
```

Setup ROIs

Regions of Interests (ROI) were defined by looking at the image intensity for both colors in an interactive widget showing the images with adjustable contrast. The ROIs are indicated with red rectangles in the widget.

[2]:
```
filename="pMHC_AL647_CELLS_AL488_*"
seq_list = [pims.open(b) for b in glob.glob(filename+".SPE")]
```

[3]:
```
topy = 0
bottomy = 154
w = 204
x_left=0
x_right=206
w2 = 225
leftroi = sdt.roi.RectangleROI((x_left,topy),(x_left+w,bottomy))
rightroi = sdt.roi.RectangleROI((x_right,topy),(x_right+w2,bottomy))
```

[4]:
```
def draw_roi(ax, roi):
    w = roi.bottom_right[0] - roi.top_left[0]
    h = roi.bottom_right[1] - roi.top_left[1]
    rect = matplotlib.patches.Rectangle(roi.
 ↪top_left,w,h,linewidth=1,edgecolor='r',facecolor='none')
    ax.add_patch(rect)
```

[5]:
```
fig, ax = plt.subplots(figsize=(5, 5))
```

[6]:
```
f= widgets.IntSlider(
    min=0,
    max=len(seq_list[0])-1,
    continuous_update=False,
    description="frame",
    value=2
    )

c= widgets.IntSlider(
    min=0,
    max=len(seq_list)-1,
    continuous_update=False,
    value=0,
    description="cell"
    )

uint16=np.iinfo(np.uint16)

v = widgets.IntRangeSlider(
    value=[180, 1337],
    min=uint16.min,
    max=uint16.max,
    continuous_update=False,
    description="contrast"
    )

v_auto = widgets.ToggleButton(value=True, description="Auto Scaling")

roi_button = widgets.ToggleButton(value=True, description="Show ROI")


def inter2(change=None):
    ax.cla()
    cell_n=c.value
    seq = seq_list[cell_n]

    if(v_auto.value):
        vmin=seq[f.value].min()
        vmax=seq[f.value].max()
    else:
        vmin, vmax = v.value

    ax.imshow(seq[f.value], cmap="gray", vmin=vmin, vmax=vmax)

    if(roi_button.value):
        draw_roi(ax, leftroi)
        draw_roi(ax, rightroi)
```

```
    fig.canvas.draw()

for w in (f, c, v, v_auto, roi_button):
    w.observe(inter2, "value")

box1 = widgets.VBox([f, c, v, v_auto, roi_button])
big_box = widgets.HBox([fig.canvas, box1])

inter2()
big_box
```

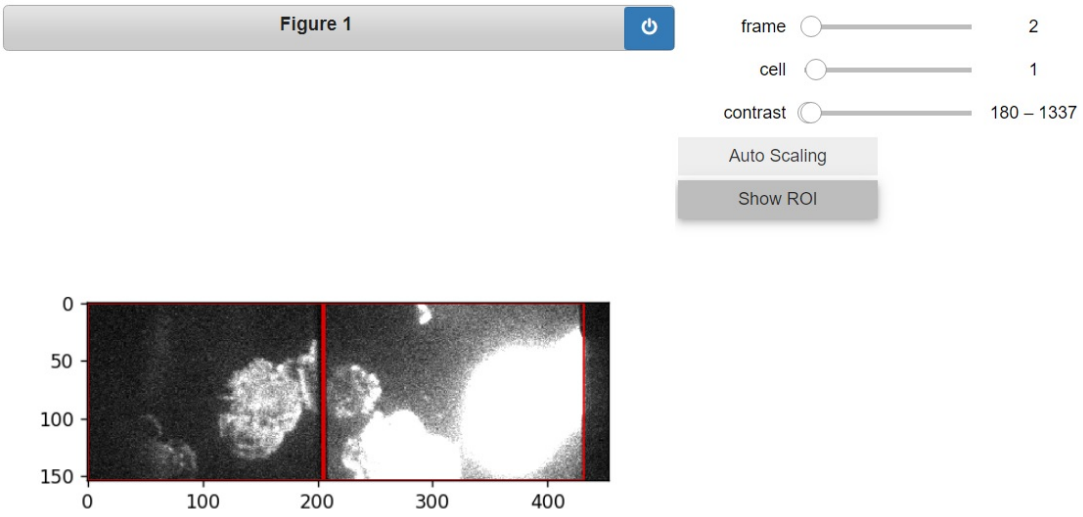

Setup Chromatic Correction

The position of TetraSpeck beads visible in both colors was used to calculate the transformation function for coordinates in one channel to coordinates in the other channel. This function is later used to correct for lateral chromatic aberrations. The plot shows that the error for the transformation is in sub-pixel range.

[7]:
```
bead_loc = [sdt.io.load(b) for b in glob.glob("beads_blau_rot*.h5")]

beads_left = [leftroi(b) for b in bead_loc]
beads_right = [rightroi(b) for b in bead_loc]
```

[8]:
```
fig2, ax2 = plt.subplots(1,2, figsize=(5, 3))
```

[9]:
```
corr = sdt.chromatic.Corrector(beads_left, beads_right)
corr.determine_parameters()
corr.test(ax=ax2)  # Plot results
```

```
fig2
```

[9]:

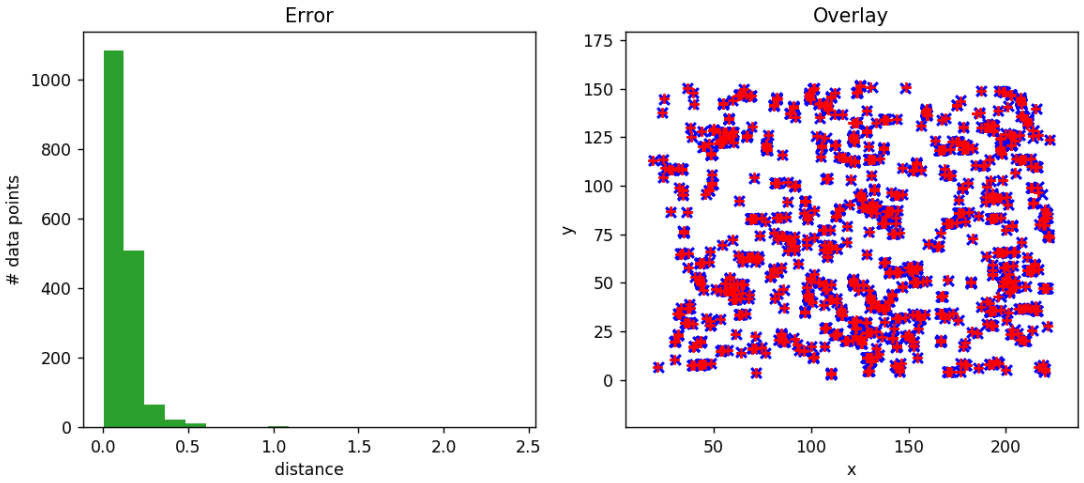

Fluorescent feature localization

An external interactive graphical user interface (sdt.gui.locator) was used to determine the parameters for the 3D-DAOSTORM algorithm and save them in *.yaml files. The fluorophores in the ROI of the frames were localized according to the illumination sequence and the parameters for 3D-DAOSTORM. These localizations were linked between frames to form trajectories using trackpy.

[10]:
```
#!python -m sdt.gui.locator
```

[11]:
```
with open('red_args.yaml', 'r') as f:
    red_args = sdt.io.yaml.load(f)

with open('blue_args.yaml', 'r') as f:
    blue_args = sdt.io.yaml.load(f)

print("blue args:")
print(blue_args['options'])
print("\nred args:")
print(red_args['options'])
```

```
blue args:
OrderedDict([('radius', 1.0), ('model', '2d'), ('threshold', 400),
('max_iterations', 20), ('find_filter', 'Cg'), ('find_filter_opts',
OrderedDict([('feature_radius', 3)])), ('min_distance', None), ('size_range',
None)])
```

```
red args:
OrderedDict([('radius', 1.0), ('model', '2d'), ('threshold', 120),
('max_iterations', 20), ('find_filter', 'Cg'), ('find_filter_opts',
OrderedDict([('feature_radius', 3)])), ('min_distance', None), ('size_range',
None)])
```

[12]:
```
seq_string = "x"+("l" + ("da" * 20)) * 2
print(seq_string)
seq_array = np.array(list(seq_string))
```

```
xldadadadadadadadadadadadadadadadadadadadaldadadadadadadadadadadadadadadadadadad
ada
```

[13]:
```
def two_color_batch(seq):
    red_seq = seq[seq_array=='a']
    blue_seq = seq[seq_array=='d']
    long_seq = seq[seq_array=='l']

    blue_locs = sdt.loc.daostorm_3d.batch_roi(blue_seq, leftroi,␣
 ↪**blue_args['options'])
    red_locs = sdt.loc.daostorm_3d.batch_roi(red_seq, leftroi,␣
 ↪**red_args['options'])

    long_locs = sdt.loc.daostorm_3d.batch_roi(long_seq, leftroi,␣
 ↪**red_args['options'])

    all_locs = pd.concat([long_locs, blue_locs, red_locs])

    return all_locs
```

[14]:
```
filename = "pMHC_AL647_CELLS_AL488*"
```

[15]:
```
#### locate and save as h5
for b in glob.glob(filename+".SPE"):
    seq = pims.open(b)

    locs = two_color_batch(seq)
    sdt.io.save(b.replace("SPE","h5"),locs)
    print(str(len(locs))+" locations saved as "+b.replace("SPE","h5"))

    track = tp.link(locs, search_range=3, memory=3)
    fn = "tracks." + b.replace("SPE","h5")
    sdt.io.save(fn, track)
    print(str(len(track))+" tracks saved as "+fn)
```

```
Frame 82: 10 trajectories present.
1084 tracks saved as tracks.pMHC_AL647_CELLS_AL488_019_.h5
```

Plot Results

The images showing the immunological synapse is overlaid with the localization and track data using the chromatic correction functioned determined previously to visualize and explore the data. It is shown using an interactive widget with adjustable options for the contrast, frame number and dataset number. Colored circles for the localizations and tracks enables the differentiation between bleed through and possible FRET events.

[16]:
```
seq_list = [pims.open(b) for b in sorted(glob.glob(filename+".SPE"))]
locs_list = [sdt.io.load(b) for b in sorted(glob.glob(filename+".h5"))]
tracks = [sdt.io.load(b) for b in sorted(glob.glob("tracks."+filename+".h5"))]
glob_list = sorted(glob.glob(filename+".SPE"))
```

[17]:
```
#filter short tracks
tracks = [tp.filter_stubs(t, threshold=3) for t in tracks]
```

[18]:
```
fig3, ax3 = plt.subplots(1,2, figsize=(10, 5))
```

[19]:
```
f= widgets.IntSlider(
    min=0,
    max=len(seq_list[0])-1,
    continuous_update=False,
    description="frame",
    value=2
    )

c= widgets.IntSlider(
    min=0,
    max=len(seq_list)-1,
    continuous_update=False,
    value=random.randint(0,len(seq_list)),
    description="cell"
    )

uint16=np.iinfo(np.uint16)

v = widgets.IntRangeSlider(
    value=[180, 1337],
    min=uint16.min,
    max=uint16.max,
    continuous_update=False,
    description="contrast"
    )

v_auto = widgets.ToggleButton(description="Auto Scaling", value=True)

locs_button = widgets.ToggleButton(description="Localizations", value=True)
track_button = widgets.ToggleButton(description="Tracks", value=True)
```

```
track_numbers_button = widgets.ToggleButton(description="Track numbering",␣
 ↪value=False)

fn_text = widgets.Text(value='Test', disabled=True)

def inter2(change=None):
    ax3[0].cla()
    ax3[1].cla()
    cell_n=c.value
    locs = locs_list[cell_n]
    seq = seq_list[cell_n]
    track = tracks[cell_n]

    fn_text.value = glob_list[cell_n]

    if(v_auto.value):
        vmin=leftroi(seq)[f.value].min()
        vmax=leftroi(seq)[f.value].max()
    else:
        vmin, vmax = v.value

    loc_of_frame = locs[locs["frame"]==f.value]
    tr_loc_of_frame = track[track["frame"]==f.value]

    for ax in ax3:
        s_bar = ScaleBar(0.160, units="um")
        ax.add_artist(s_bar)
        ax.axis("off") #remove all axis labels etc.

    if(locs_button.value):
        ax3[0].scatter(loc_of_frame["x"], loc_of_frame["y"], marker="o",␣
 ↪edgecolor="y", s=100, facecolor="none",)
        ax3[1].scatter(loc_of_frame["x"], loc_of_frame["y"], marker="o",␣
 ↪edgecolor="y", s=100, facecolor="none",)
    #if(track_button.value):
    #   color_seq = plt.cm.Set2.
    #    ax3[0].scatter(tr_loc_of_frame["x"], tr_loc_of_frame["y"], marker="o",␣
 ↪edgecolor=color_seq, s=100, facecolor="none",)
    if(track_button.value):
        #color_seq = plt.cm.Paired.colors
        color_seq = ["b", "r", "c", "m", "w", "xkcd:lime", "xkcd:dark red",␣
 ↪"xkcd:bright purple",
                     "xkcd:mint green", "xkcd:light red"]
        for index, p in tr_loc_of_frame.iterrows():
            p_number = int(p['particle'])
            color = color_seq[(p_number%len(color_seq))]
```

```
            ax3[0].scatter(p["x"], p["y"], marker="o", edgecolor=color, s=100,␣
 ↪facecolor="none",)
            ax3[1].scatter(p["x"], p["y"], marker="o", edgecolor=color, s=100,␣
 ↪facecolor="none",)

    if(track_numbers_button.value):
        for index, p in tr_loc_of_frame.iterrows():
            xy=p[["x", "y"]]
            xy = xy + (4,10)
            ax3[0].annotate(str(int(p['particle'])), xy=xy, color='r')

    ax3[0].imshow(leftroi(seq[f.value]), cmap="gray", vmin=vmin, vmax=vmax)
    ax3[1].imshow(corr(rightroi(seq[f.value]),channel=2), cmap="gray")

    fig3.canvas.draw()

for w in (f, c, v, v_auto, locs_button, track_button, track_numbers_button):
    w.observe(inter2, "value")

box1 = widgets.HBox([f, c, v, v_auto])
box2 = widgets.HBox([fn_text, locs_button, track_button, track_numbers_button])
big_box = widgets.VBox([fig3.canvas, box1, box2])

inter2()
big_box
```

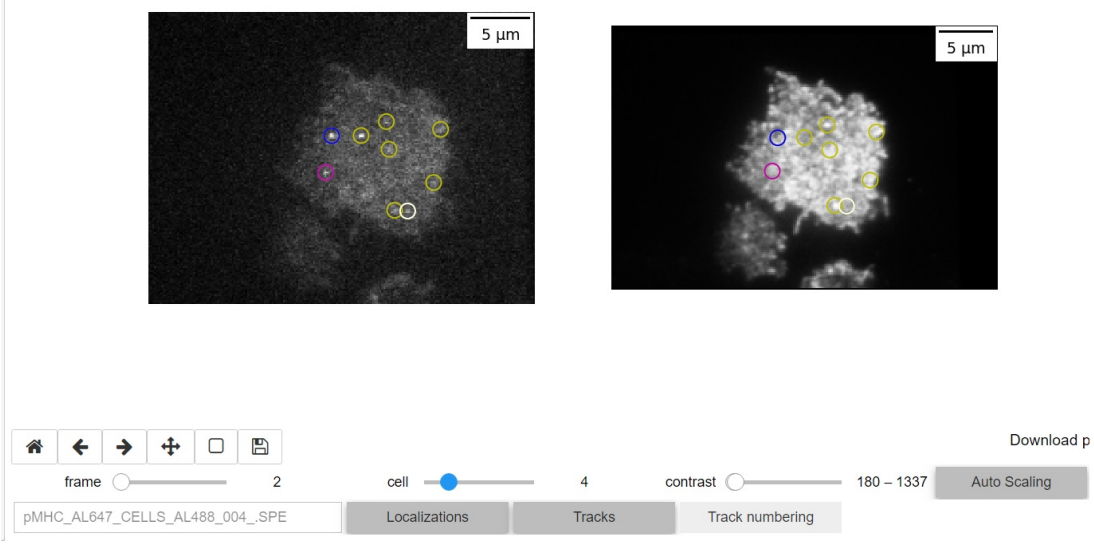

[20]:
```
fig3.savefig("2018.03.26_pMHC_AL647_CELLS_AL488_009_acc.png")
```

Bibliography

[1] Johannes B Huppa, Markus Axmann, Manuel A Mörtelmaier, Björn F Lillemeier, Evan W Newell, Mario Brameshuber, Lawrence O Klein, Gerhard J Schütz, and Mark M Davis. "TCR–peptide–MHC interactions in situ show accelerated kinetics and increased affinity". In: *Nature* 463.7283 (2010), p. 963 (cit. on pp. ii, iii, 2, 14, 17–19, 24, 25, 34).

[2] Geoff P O'Donoghue, Rafal M Pielak, Alexander A Smoligovets, Jenny J Lin, and Jay T Groves. "Direct single molecule measurement of TCR triggering by agonist pMHC in living primary T cells". In: *Elife* 2 (2013), e00778 (cit. on pp. ii, iii, 2, 17–19, 24, 25).

[3] Darrell J Irvine, Marco A Purbhoo, Michelle Krogsgaard, and Mark M Davis. "Direct observation of ligand recognition by T cells". In: *Nature* 419.6909 (2002), p. 845 (cit. on p. 1).

[4] Medinaz. *Antigen Presenting Cells - Few basic differences*. Youtube. 2018. URL: https://www.youtube.com/watch?v=XekCo6DRC4k&t=41s (cit. on p. 1).

[5] Timothy W McKeithan. "Kinetic proofreading in T-cell receptor signal transduction". In: *Proceedings of the national academy of sciences* 92.11 (1995), pp. 5042–5046 (cit. on p. 2).

[6] Joshua D Rabinowitz, Craig Beeson, Daniel S Lyons, Mark M Davis, and Harden M McConnell. "Kinetic discrimination in T-cell activation". In: *Proceedings of the National Academy of Sciences* 93.4 (1996), pp. 1401–1405 (cit. on p. 2).

[7] K.M. Murphy and C. Weaver. *Janeway's Immunobiology*. Garland Science/Taylor & Francis Group, LLC, 2016. ISBN: 9780815345053. URL: https://books.google.at/books?id=YH1djwEACAAJ (cit. on p. 2).

[8] Bi-Chang Chen, Wesley R Legant, Kai Wang, Lin Shao, Daniel E Milkie, Michael W Davidson, Chris Janetopoulos, Xufeng S Wu, John A Hammer, Zhe Liu, et al. "Lattice light-sheet microscopy: imaging molecules to embryos at high spatiotemporal resolution". In: *Science* 346.6208 (2014), p. 1257998 (cit. on p. 6).

[9] Anne S Ulrich, Malkit Sami, and Anthony Watts. "Hydration of DOPC bilayers by differential scanning calorimetry". In: *Biochimica et Biophysica Acta (BBA)-Biomembranes* 1191.1 (1994), pp. 225–230 (cit. on p. 8).

[10] E. Hecht. *Optics, Global Edition*. Pearson Education Limited, 2016. ISBN: 9781292096964 (cit. on p. 11).

[11] Hellen C Ishikawa-Ankerhold, Richard Ankerhold, and Gregor PC Drummen. "Advanced fluorescence microscopy techniques—Frap, Flip, Flap, Fret and flim". In: *Molecules* 17.4 (2012), pp. 4047–4132 (cit. on pp. 15, 16).

[12] Achillefs N. Kapanidis, Ted A. Laurence, Nam Ki Lee, Emmanuel Margeat, Xiangxu Kong, and Shimon Weiss. "Alternating-Laser Excitation of Single Molecules". In: *Accounts of Chemical Research* 38.7 (2005). PMID: 16028886, pp. 523–533. DOI: 10.1021/ar0401348 (cit. on p. 14).

[13] *The Jupyter Notebook*. URL: http://jupyter.org/ (visited on 10/10/2017) (cit. on p. 22).

[14] Hazen Babcock, Yaron M. Sigal, and Xiaowei Zhuang. "A high-density 3D localization algorithm for stochastic optical reconstruction microscopy". In: *Optical Nanoscopy* 1.1 (July 2012), p. 6. ISSN: 2192-2853. DOI: 10.1186/2192-2853-1-6. URL: https://doi.org/10.1186/2192-2853-1-6 (cit. on p. 23).

[15] Daniel Allan, Thomas Caswell, Nathan Keim, and Casper van der Wel. *trackpy: Trackpy v0.3.2*. Aug. 2016. URL: http://github.com/soft-matter/trackpy/ (cit. on p. 23).

[16] Sungchul Hohng, Chirlmin Joo, and Taekjip Ha. "Single-molecule three-color FRET". In: *Biophysical journal* 87.2 (2004), pp. 1328–1337 (cit. on p. 24).